Organic Geochemistry 164 (2022) 104349

Contents lists available at ScienceDirect

Organic Geochemistry

journal homepage: www.elsevier.com/locate/orggeochem

Lipid biomarkers in Lake Wudalianchi record abrupt environmental changes from the volcanic eruption in 1776

Yuan Yao [a,b,c,*], Yongsong Huang [c,*], Jiaju Zhao [b], Li Wang [d], Hai Cheng [a,b,e]

[a] Institute of Global Environmental Change, Xi'an Jiaotong University, Xi'an 710054, China
[b] State Key Laboratory of Loess and Quaternary Geology, Institute of Earth Environment, Chinese Academy of Sciences, Xi'an 710061, China
[c] Department of Earth, Environmental and Planetary Sciences, Brown University, Providence, RI 02912, USA
[d] State Key Laboratory of Organic Geochemistry, Guangzhou Institute of Geochemistry, Chinese Academy of Sciences, Guangzhou 510640, China
[e] Key Laboratory of Karst Dynamics, Ministry of Land and Resources, Institute of Karst Geology, Chinese Academy of Geological Sciences, Guilin 541004, China

ARTICLE INFO

Associate Editor – **Julian Sachs**

Keywords:
Lipid biomarkers
Volcanic eruption
Alkenones
GDGTs
Methane cycling
Volcanic lakes

ABSTRACT

Volcanic eruptions can cause abrupt changes in surrounding environments, but detailed sediment records of such changes are rare. The very high sediment accumulation rate in Lake Wudalianchi, a volcanic-dammed freshwater lake in northeastern China, provides an excellent opportunity for reconstructing volcanic-induced environmental change. Here we use multiple lipid biomarkers to reconstruct changes in aquatic ecosystems, hydrology, and methane cycling before and after a regional explosive volcanic eruption in 1776. Our results indicate that the Wudalianchi catchment was a shallow organic-rich marsh environment with abundant aquatic emergent macrophytes and an intense microbial methane cycle before the volcanic eruption. Following the volcanic eruption, the marsh was rapidly transformed into an oligohaline lake environment due to river channel damming by lava. Associated with the abrupt environmental change, we observe corresponding changes of cyclisation ratios of branched glycerol dialkyl glycerol tetraethers or brGDGTs (CBT and CBT′ indices), and the inferred pH displays an abrupt increase of ~1.3. Group 1 alkenones emerge abruptly after the eruption when the inferred pH exceeds 8. Our results provide the first high-resolution reconstruction of environmental change induced by volcanic eruption and demonstrate the high efficacy of the lipid biomarkers in recording aquatic and terrestrial changes.

1. Introduction

Inland surface water systems, including wetlands, rivers and lakes, cover ~ 9% (~11.7 × 10^6 km^2) of the global ice-free land surface (Lehner and Döll, 2004). They provide suitable habitats for many aquatic organisms (Johnson et al., 2001) and contribute substantially to global biogeochemical cycling, especially methane cycles (Reay et al., 2018). However, these ecosystems and associated biogeochemical cycling are extremely sensitive to changes in environmental conditions, such as catchment morphology, hydrology, and nutrients (Carpenter et al., 2011; Markovic et al., 2017). In particular, natural disaster events, such as volcanic eruptions, can lead to an abrupt shift in the ecosystem (Kilian et al., 2006; Payne and Egan, 2019).

Volcanic eruptions frequently occur worldwide, with 869 confirmed Holocene eruptions and 40–50 ongoing eruptions at any given time (Siebert and Simkin, 2013). The explosive events can greatly affect the environmental conditions of regional hydrology by releasing high-temperature lava and subsequent rapid weathering of basalt and tephra (Kilian et al., 2006; Payne and Egan, 2019). Lake Wudalianchi, the second largest volcanic-dammed lake in China, was formed due to the lava flows partially blocking the river channel during the explosive eruption of Laoheishan volcano in 1776 (Fig. 1b,c). The Wudalianchi magma was generated by a hydrous mantle upwelling from the mantle transition zone, and the resulting basalts feature extremely high potassium (K) and sodium (Na) contents with high alkalinity (Kuritani et al., 2013; Sun et al., 2019). However, there have been no previous studies on Wudalianchi biogeochemical changes before and after volcanic eruption.

There have been major advances in lipid biomarker proxies for reconstructing hydrological and biogeochemical changes. For example, Group 1 alkenones and alkenone isomer-based RIK_{37} (ratio of isomeric ketones of C_{37} chain length; Longo et al., 2016) index can be successfully

* Corresponding authors at: Institute of Global Environmental Change, Xi'an Jiaotong University, Xi'an 710054, China (Y. Yao). Department of Earth, Environmental and Planetary Sciences, Brown University, Providence, RI 02912, USA (Y. Huang).
E-mail addresses: yaoyuan@xjtu.edu.cn (Y. Yao), yongsong_huang@brown.edu (Y. Huang).

https://doi.org/10.1016/j.orggeochem.2021.104349
Received 1 September 2021; Received in revised form 20 November 2021; Accepted 1 December 2021
Available online 8 December 2021

used to infer past salinity changes in freshwater and oligohaline environments (Yao et al., 2020a, 2021; Huang et al., 2021). Based on empirical correlations, cyclization indices (CBT and CBT′) of bacterial-derived branched glycerol dialkyl glycerol tetraethers (brGDGTs) have been proposed as the indicators of pH changes (Weijers et al., 2007; Tierney and Russell, 2009; Castañeda and Schouten, 2011; De Jonge et al., 2014). The CBT index has been applied to some lake sediment records to infer past lake water pH changes (e.g., Tyler et al., 2010; Cao et al., 2017), but the sensitivity of the proxy, especially in the case of abrupt change caused by a volcanic eruption, remains to be tested.

The Methane Index (MI; Zhang et al., 2011) based on archaeal-derived isoprenoid GDGTs (iGDGTs) has been proposed to trace anaerobic oxidation of methane (AOM) as an indicator of methane-rich environments in ocean (Zhang et al., 2011), but its applicability and consistency in lake and marsh/peatland environments is still to be verified.

A consortium of multiple biomarker proxies (also including bacterial-derived diploptene $\delta^{13}C$, *n*-alkane-based on P_{aq} and carbon preference index (CPI)) can be used to explore biogeochemical changes at Wudalianchi throughout the 1776 volcanic eruption. The Wudalianchi records also provide an excellent opportunity to test the sensitivity/efficacy of a full consortium of biomarker proxies in the context of abrupt environmental change caused by a volcanic eruption.

Here we present a multi-proxy record of lipid biomarkers, including alkenones, GDGTs, *n*-alkanes, and diploptene, in a sediment core cutting across the tephra layer resulting from the 1776 eruption at Lake Wudalianchi, northeastern China. Our main objectives are to: (1) explore the depositional environments of Wudalianchi before and after the volcanic eruption; (2) take advantage of high-amplitude, abrupt environmental change induced by the explosive volcanic eruption to test the sensitivity, response time, and consistency of various lipid biomarker proxies in recording changes in biogeochemical cycles and aquatic pH, as well as aquatic and terrestrial productivities.

2. Material and methods

2.1. Study site and samples

Lake Wudalianchi (48°40′N–48°47′N; 126°06′E–126°15′E), located in the northwest of Heilongjiang Province in northeastern China (Fig. 1a), is currently a freshwater lake with relatively high pH (salinity and pH measured on July 2016 were 0.09 ppt and 8.6, respectively; Yao et al., 2019). The Wudalianchi volcanic field covers an area of ~ 720 km^2, and the latest explosive volcanic eruption occurred in 1776 (Laoheishan eruption; Sun et al., 2019). During the volcanic eruption, the Shilong River was partially blocked by lava flows, which formed five hydrologically connected lakes (Wudalianchi Pool 1, Pool 2, Pool 3, Pool 4, and Pool 5; Fig. 1b,c). At present, there are two river inflows into and one river outflow from Lake Wudalianchi (Supplementary Fig. S1). The regional lake water flows southward, due to higher elevations in the north, east, and west of Wudalianchi region. The mean annual air temperature of the Wudalianchi region during 1979–2013 is ~ 0.4 °C, with the warmest season (June-August) mean air temperature being 18.7 °C (http://chelsa-climate.org/, Version1.2) (Karger et al., 2017). The mean annual precipitation during 1979–2013 was ~530 mm (http://chelsa-climate.org/, Version1.2) (Karger et al., 2017).

An 82 cm long sediment core was retrieved from the center of Lake Wudalianchi Pool 2 at a water depth of ~ 11 m on March 20, 2018 (Supplementary Fig. S1) using a gravity corer (Yao et al., 2021). Between ~ 65–69 cm depth, the sediments are dominated by dark grey tephra deposits (Supplementary Fig. S2), resulting from the most recent volcanic eruption event in 1776 (Yao et al., 2021). The sediments between 69 cm and 82 cm depth were retained in the metal drill bit of gravity corer. The sediment core above 69 cm was sub-sampled at 0.5 cm intervals, and the samples below 69 cm were sub-sampled at 1 cm intervals. All collected samples were frozen at − 20 °C in the laboratory until analysis.

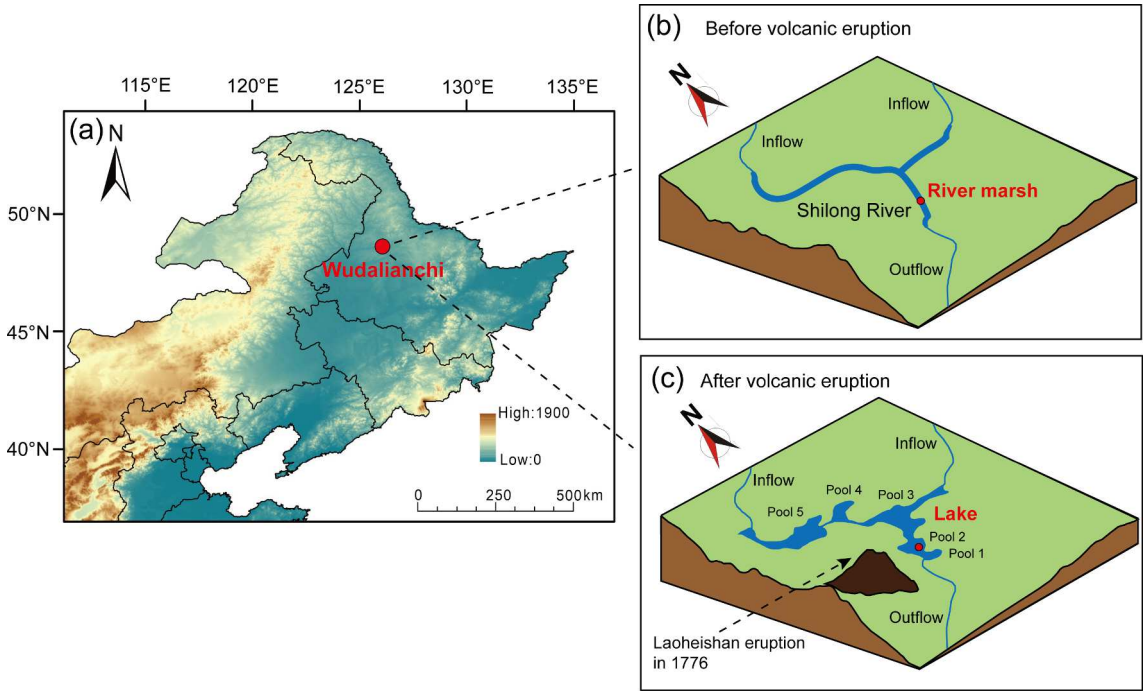

Fig. 1. (a) Location of Lake Wudalianchi on a topographic map. (b, c) Schematic diagrams illustrating changes in Wudalianchi catchment before and after the volcanic eruption in 1776 (red circle shows location of the Wudalianchi sediment core in this study). (For interpretation of the references to colour in this figure legend, the reader is referred to the web version of this article.)

2.2. Analytical methods

All sediment samples were freeze-dried and extracted by sonication (3 ×) with dichloromethane (DCM)/methanol (MeOH) (9:1, v/v). The extracts were purified by column chromatography with silica gel using *n*-hexane, DCM, and MeOH, respectively. Alkenones in the DCM fractions were analyzed with an Agilent 7890 N gas chromatography system equipped with a flame ionization detector (GC-FID) and a Restek Rtx-200 GC column (105 m × 250 μm × 0.25 μm film thickness) (Zheng et al., 2017). The following GC-FID oven program was used: initial temperature of 50 °C (hold 2 min), ramp 20 °C/min to 255 °C, ramp 3 °C/min to 320 °C (hold 25 min). Diploptene and *n*-alkanes in the hexane fractions was analyzed by gas chromatography–mass spectrometry (GC–MS; Thermo Fisher Scientific), and the diploptene $\delta^{13}C$ values were analyzed using a Trace GC Ultra^{TM} (Thermo Scientific) coupled via a combustion reactor to a Delta V Advantage isotope ratio mass spectrometer (Thermo Scientific). The following GC oven program was used: initial temperature of 80 °C (hold 2 min), ramp 3 °C/min to 300 °C (hold 10 min). The $\delta^{13}C$ values are reported relative to the Vienna Pee Dee Belemnite (VPDB) standard ($\delta^{13}C = [(R_{sample} - R_{standard})/R_{standard}] \times 1000$; where R is the $^{13}C/^{12}C$ ratio), and the analytical error was ± 0.3‰. The reproducibility and accuracy for diploptene $\delta^{13}C$ values were evaluated by measuring *n*-alkane standards (C_{21}, C_{25}, C_{27}, C_{29}, C_{31}, and C_{33} *n*-alkanes) between every five measured samples.

GDGTs in the MeOH fractions were analyzed using high performance liquid chromatography coupled to atmospheric pressure chemical ionization-mass spectrometry (HPLC–APCI-MS) with a Shimadzu LC-MS 8030. We followed the method reported in De Jonge et al. (2014) and Hopmans et al. (2016) to analyze 5-methyl and 6-methyl brGDGTs. Specifically, normal phase HPLC separation was achieved by coupling two Inertsil SIL-100A silica columns (250 mm × 4.6 mm, 3 μm; GL Sciences Inc.), using a linear gradient of isopropanol and *n*-hexane, starting with 97% hexane and decreasing to 95% hexane in 85 min. The column was thereafter cleaned with 90% A for 20 min after each injection. Scanning was performed in selected ion monitoring (SIM) mode to target specific *m/z* values for each GDGT compounds (GDGT-0 (1302), GDGT-1 (1300), GDGT-2 (1298), GDGT-3 (1296), crenarchaeol and its regioisomer (1292), and 15 brGDGTs (IIIa (1050), IIIa′ (1050), IIIb (1048), IIIb′ (1048), IIIc (1046), IIIc′ (1046), IIa (1036), IIa′ (1036), IIb (1034), IIb′ (1034), IIc (1032), IIc′ (1032), Ia (1022), Ib (1020), and Ic (1018)).

The major and trace elements of the solvent-extracted sediment residuals were analyzed with an Energy Dispersive X-Ray Fluorescence (ED-XRF) spectrometer Epsilon 5. The total organic carbon (TOC) and total nitrogen (TN) contents of the sediment residuals after removing carbonates with 2 M HCl were measured on a Vario EL III elemental analyzer. The analytical errors were < ±0.05%.

The data for diploptene and its $\delta^{13}C$ values, GDGTs (iGDGT-0 flux and GDGT-0/crenarchaeol), TOC, and TN in the uppermost 21 cm (~1950–2010) sediments have been recently reported by Yao et al. (2021). In this study, we focus on the sedimentary interval at 30–82 cm depth to address volcanic-induced environmental changes.

2.3. Biomarker indices

The alkenone isomer-based RIK_{37} index (Longo et al., 2016) is calculated as

$$RIK_{37} = \frac{[C_{37:3a}]}{[C_{37:3a} + C_{37:3b}]} \quad (1)$$

where the "a" and "b" subscripts refer to the $\Delta^{7,14,21}$ and $\Delta^{14,21,28}$ tri-unsaturated alkenones, respectively.

The P_{aq} uses *n*-alkanes to evaluate the relative inputs of emergent and submerged/floating aquatic macrophytes, and terrestrial plants (Ficken et al., 2000), and is calculated as

$$P_{aq} = \frac{C_{23} + C_{25}}{C_{23} + C_{25} + C_{29} + C_{31}} \quad (2)$$

The CPI for *n*-alkanes is calculated as

$$CPI = \frac{C_{25} + C_{27} + C_{29} + C_{31} + C_{33}}{C_{24} + C_{26} + C_{28} + C_{30} + C_{32}} \times 0.5 \quad (3)$$

The MI can be used to trace archaeal methanotrophy (Zhang et al., 2011), and is calculated using GDGT isomers as

$$MI = \frac{GDGT\text{-}1 + GDGT\text{-}2 + GDGT\text{-}3}{GDGT\text{-}1 + GDGT\text{-}2 + GDGT\text{-}3 + Crenarchaeol + Crenarchaeol'} \quad (4)$$

The cyclisation ratios of brGDGTs (CBT and CBT′) are calculated according to Weijers et al. (2007) and De Jonge et al. (2014), and are used to trace water pH changes.

$$CBT = -\log\frac{Ib + IIb + IIb'}{Ia + IIa + IIa'} \quad (5)$$

$$CBT' = \log\frac{Ic + IIa' + IIb' + IIc' + IIIa' + IIIb' + IIIc'}{Ia + IIa + IIIa} \quad (6)$$

The methylation of 5-methyl brGDGTs (MBT'_{5Me}) is calculated according to De Jonge et al. (2014).

$$MBT'_{5Me} = \frac{Ia + Ib + Ic}{Ia + Ib + Ic + IIa + IIb + IIc + IIIa} \quad (7)$$

2.4. Statistical analyses

Principal components analysis (PCA) was performed to investigate the differences in brGDGT distributions from our sediment core and regional surface soils using the Canoco software version 4.5.

3. Results and discussion

3.1. Records of major and trace elemental compositions

In our sediment core from Lake Wudalianchi, we observe a ~ 4 cm-thick tephra layer with a mixture of mud and volcanic ash particle at ~ 65–69 cm depth (Supplementary Fig. S2), which may capture the most recent explosive eruption event of Laoheishan volcano in 1776 (Chen, 1994; Sun et al., 2019). The eruption event date (1776) was established by historical accounts (Chen, 1994). The same tephra layers in the regional lakes (e.g., Lake Nangelaqiushan; ~14 km west of the Lake Wudalianchi) have also been reported in the previous studies as well (e.g., Sun et al., 2019). In addition, based on the ^{210}Pb and ^{137}Cs dating of the sediment core (Yao et al., 2021), the sedimentation rate above the tephra is on average ~ 0.283 cm/yr. Assuming a relatively constant sedimentation rate above the tephra, the age at 65 cm depth of top tephra would be ~ 1780, which is very close to the time of the most recent explosive eruption from Laoheishan volcano in 1776 (Chen, 1994; Sun et al., 2019). The basalt and tephra from the volcanic eruption contains abundant alkaline volcanic glass shards with highly enriched K and Na (Kuritani et al., 2013; McGee et al., 2015; Sun et al., 2019). The alkaline metal oxide contents (total K_2O and Na_2O contents; ~11 wt%) are exceptionally high compared to Quaternary tephras in other region of northeastern China (~5–7 wt% for most samples; Sun et al., 2019), Japan (~8 wt%; Maruyama et al., 2016), North America (~9 wt%; Maruyama et al., 2016), Iceland (~5–8 wt%; Tomlinson et al., 2015), Greece (~5–8 wt%; Tomlinson et al., 2015), and global seafloor (~3 wt %; Melson et al., 2002). These contents are similar to the volcanic glass found from anorogenic tephra in Pantelleria (Italy) and Terceira (Azores) (Tomlinson et al., 2015) as well as from post subduction tephra in Colli Albani (Italy) (Cross et al., 2014) and Western Anatolia (Turkey) (Tomlinson et al., 2015). Moreover, the Wudalianchi basalt and tephra (Supplementary Fig. S3) also contains abundant Mg, Ti, Ba, and Zr

(Supplementary Table S1; McGee et al., 2015).

We analyzed the major and trace elements in our Lake Wudalianchi sediment core (Fig. 2). The K_2O, MgO, Na_2O, Ti, Ba, and Zr concentrations increase abruptly by 3–4 fold at 65–69 cm depth relative to those before the volcanic eruption (>69 cm depth) (Fig. 2), clearly marking the tephra deposition during the eruption event of Laoheishan volcano in 1776. Based on the elemental composition data, we divide our sediment record into three units: pre- (> 69 cm), syn- (65–69 cm), and post-eruption (< 65 cm) phases (Fig. 2). After the eruption, concentrations of these elements decrease slowly from about 64 cm to 55 cm depth, reaching approximately constant concentrations between 55 cm and 30 cm depth. The concentrations in the post-eruption phase are higher than those in the pre-eruption phase, which reflects a continuous process of the element supply from the surrounding basalt and tephra due to their progressive weathering and transport.

3.2. Depositional environment of Wudalianchi prior to volcanic eruption

We recovered 82 cm of Wudalianchi sediment record beyond the tephra layer (Supplementary Fig. S2), indicating that Wudalianchi was already accumulating sediment. The sediments in the pre-eruption phase consist of light brown-coloured mud with abundant plant debris (Supplementary Fig. S4a,b), whereas the sediment mud in the post-eruption phase is light grey (Supplementary Fig. S4d). However, there have been no previous studies on the nature of the depositional environmental prior to the Laoheishan eruption in 1776. Our following geochemical evidence, including nature of the sediment (described above), *n*-alkane distributions, high TOC and TN, and a series of biomarker proxies of microbial methane cycling (Fig. 3), indicate that the environment was a shallow organic-rich river marsh prior to the volcanic eruption.

The *n*-alkane-based P_{aq} (Eq. (2)) has been used to infer aquatic macrophyte contributions, with the values of 0.1–0.4 corresponding to emergent macrophytes (Ficken et al., 2000). Most of the emergent macrophytes and their biomass are closely associated with shallow marsh environment (e.g., Vis et al., 2003). In the pre-eruption phase, P_{aq} values are ~ 0.2 and C_{23}–C_{33} *n*-alkanes have very high concentrations (average value: 5.8 μg/g; Fig. 3a), likely reflecting inputs from emergent aquatic macrophytes associated with a shallow marsh environment, as well as high biomass or low rate of organic decomposition in waterlogged, cool conditions. After the volcanic eruption, P_{aq} values are relatively high with the average of 0.51, and C_{23}–C_{33} *n*-alkane concentrations substantially decrease by ~ 16 fold (Fig. 3a). The data indicate shifts in the relative contribution of *n*-alkane sources (e.g., increase in contributions from aquatic macrophyte and/or mosses), faster degradation of *n*-alkanes or less terrestrial plant inputs. Lower CPI (Eq. (3)) values in the lake phase than in the marsh phase (Fig. 3a) may indicate greater biodegradation of plant-derived *n*-alkanes and more contribution from aerobic microbes (Chen et al., 2019, 2021).

The sediments in the pre-eruption phase contain very high TOC and TN contents with average values of 21.4% and 1.7%, respectively, which are followed by a substantial decrease, by ~ 9 fold, after the volcanic eruption (Fig. 3b). In northeastern China, the common ranges of TOC and TN contents in lake sediments are ~ 1–7% and ~ 0.05–0.6%, respectively (e.g., Mackenzie et al., 2018; Bao et al., 2021), whereas ombrotrophic peatland environments have very high TOC and TN (common ranges: ~30–40% for TOC; ~0.6–2.3% for TN; e.g., Bao et al., 2016; Liu et al., 2018), with modern marshes having an intermediate trophic level (common ranges: ~5–25% for TOC; ~0.3–1.8% for TN; e.g., Lyu et al., 2016). The TOC and TN contents in the pre-eruption phase sediments are within the common range found in the marsh environments in the northeastern China.

Organic-rich marsh environments often facilitate high microbial activities of methanogenesis and methanotrophy (e.g., Megonigal, 2002; Bridgham et al., 2013). All known methanogens involved in microbial methanogenesis are affiliated to the Euryarchaeota group belonging to the Archaea (Borrel et al., 2011). The GDGT-0/crenarchaeol ratio can be applied as a proxy for evaluating the relative contribution of methanogenic Euryarchaeota, with the value of > 2 indicating a substantial abundance of methanogenic Euryarchaeota (Blaga et al., 2009; Naeher et al., 2014). On the other hand, MI (Eq. 4) and diploptene $\delta^{13}C$ values can be used to trace archaeal and bacterial methanotrophy, respectively (Zhang et al., 2011; Pancost and Sinninghe Damsté, 2003). Higher MI, especially the value > 0.5, indicates an increased abundance of

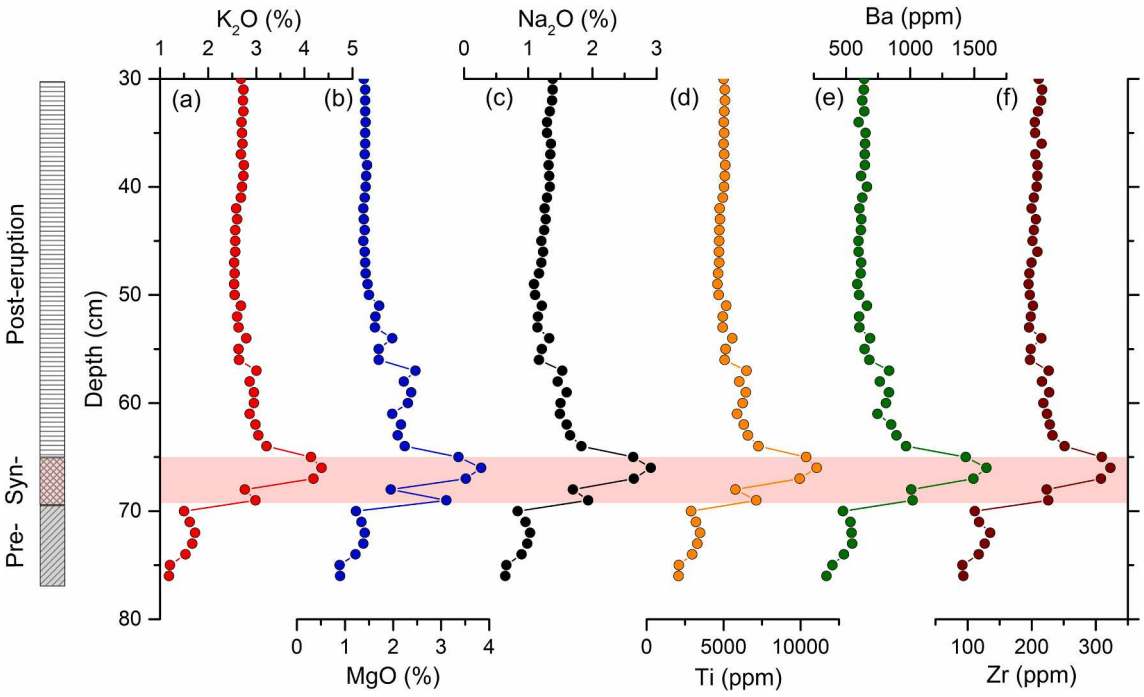

Fig. 2. Depth variations in K_2O, MgO, Na_2O, Ti, Ba, and Zr in our Lake Wudalianchi sediment core. Red shaded area represents *syn*-eruption phase from 65 cm to 69 cm depth. (For interpretation of the references to colour in this figure legend, the reader is referred to the web version of this article.)

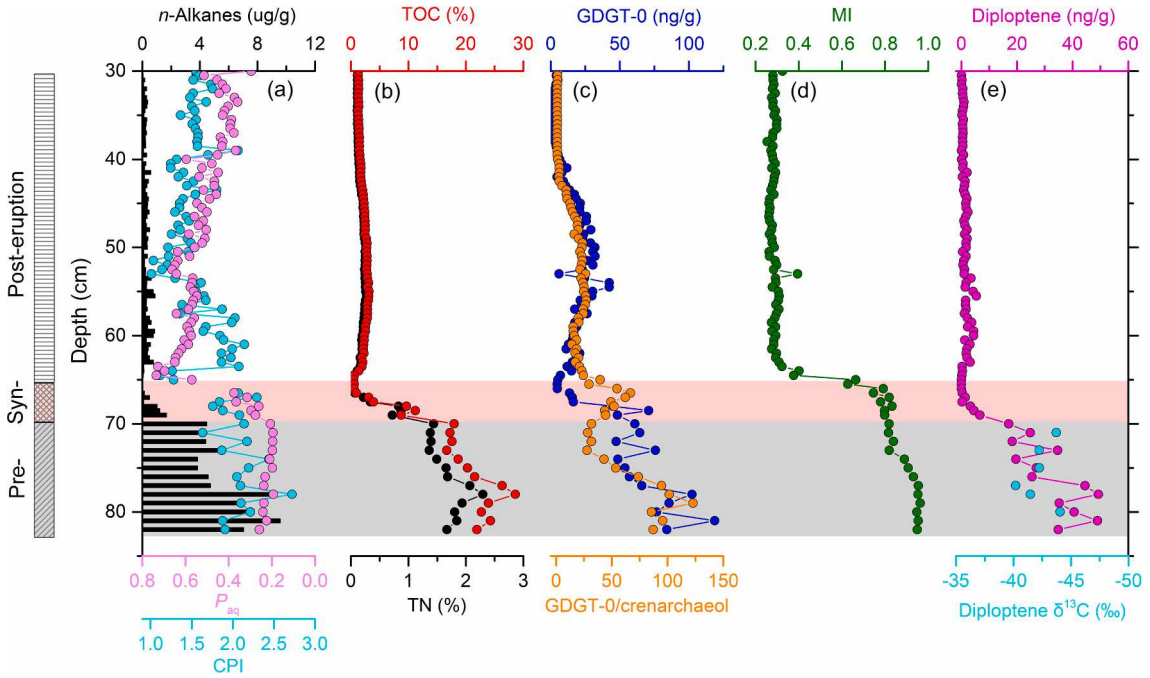

Fig. 3. Comparison of methane cycling with environment conditions from our Lake Wudalianchi sediment core along depth variation. (a) C_{23}–C_{33} *n*-alkane concentration (relative to sediment weight), CPI, and P_{aq}, (b) TOC and TN, (c) GDGT-0 concentration (relative to sediment weight) and GDGT-0/crenarchaeol, (d) MI, (e) diploptene concentration (relative to sediment weight) and $\delta^{13}C$ values (after the volcanic eruption, concentrations of diploptene are too low to permit carbon isotope measurements). Grey shaded area represents pre-eruption period of depth range from 69 cm to 82 cm; Red shaded area represents *syn*-eruption phase from 65 cm to 69 cm depth. (For interpretation of the references to colour in this figure legend, the reader is referred to the web version of this article.)

methanotrophic Euryarchaeota normally associated with gas hydrates and/or CH_4-rich environments (Zhang et al., 2011). Low diploptene $\delta^{13}C$ values (< –40‰) are often associated with the consumption of ^{13}C-depleted biogenic CH_4 by the methanotrophic bacterial community (e.g., Pancost and Sinninghe Damsté, 2003). Thus, an increase in the concentration of diploptene with low $\delta^{13}C$ values has been associated with an increase in bacterial methanotrophic contributions in natural environments, including marine cold seeps (Pancost and Sinninghe Damsté, 2003), peatlands (Zheng et al., 2014; Inglis et al., 2019), and lakes (Elvert et al., 2016; Yao et al., 2021).

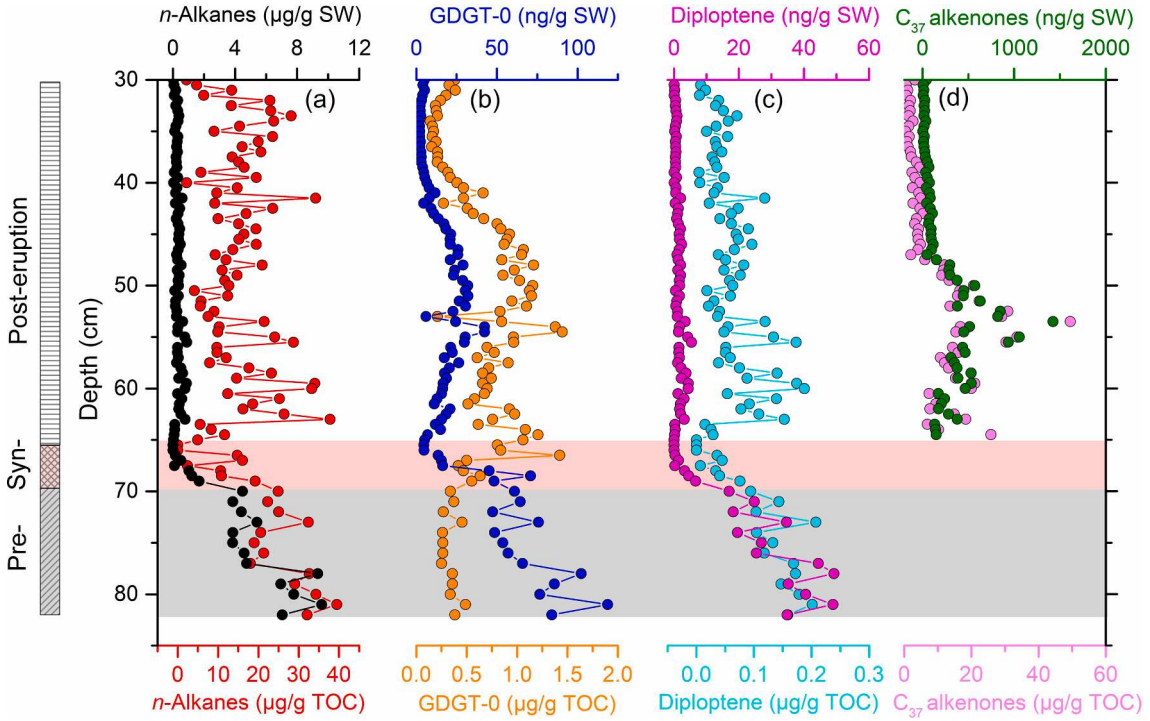

Fig. 4. Depth variations in concentrations of C_{23}–C_{33} *n*-alkanes, GDGT-0, diploptene, and C_{37} alkenones relative to sediment weight (SW) and total organic matter (TOC).

Prior to the volcanic eruption, GDGT-0/crenarchaeol ratios and GDGT-0 concentrations are extremely high, with average values of 67.5 ng/g and 72.4 ng/g, respectively (Fig. 3c), indicating enhanced archaeal methanogenesis. MI values range from 0.82 to 0.96, which falls within "methane impacted" environments (gas hydrates and/or CH_4-rich environments; Zhang et al., 2011) (Fig. 3d). This may reflect highly enhanced archaeal methanotrophy with the predominance of methanotrophic Euryarchaeota (Zhang et al., 2011). The diploptene concentration is also extremely high with an average value of 32.3 ng/g, and the diploptene $\delta^{13}C$ is very depleted with an average value of –42.3‰ (Fig. 3e), indicating enhanced bacterial methanotrophy. Overall, the intense microbial activities of methanogenesis and methanotrophy in the pre-eruption phase support a shallow organic-rich marsh environment.

We also compared the downcore trends in biomarker concentrations (including *n*-alkanes, GDGT-0, diploptene, and C_{37} alkenones) relative to sediment weight and relative to TOC (Fig. 4). The biomarker concentrations relative to sediment weight show a major contrast between the marsh and lake phases, with the marsh phase having significantly higher concentrations. This could be readily explained by: (1) high productivity from vascular plants in the marsh phase, as demonstrated by the high concentration of long-chain *n*-alkanes as well as abundant vascular plant debris (Supplementary Fig. S4a,b); and (2) more anaerobic condition in the marsh phase which facilitates preservation of organic matter. High organic contents and anaerobic conditions in the marsh phase promote methanogenesis and methanotrophy, which is reflected by the high concentrations of GDGT-0 as well as diploptene (Fig. 4).

Normalization to TOC appears to reduce the contrast between the concentrations of *n*-alkanes and diploptene between the pre-eruption marsh phase and post-eruption lake phase. However, both long-chain *n*-alkanes and diploptene still display higher TOC-normalized concentrations in the marsh phase, suggesting that productivities of vascular plants and methanotrophic bacteria relative to other organisms are higher in the marsh phase than in the lake phase. In addition, relatively high concentrations of diploptene are also observed between 50 cm and 65 cm depth during the lake phase, coinciding approximately with a prominent peak of alkenone concentrations (Fig. 4). This suggests that higher algal productivity during this interval may have promoted the activities of methanotrophic bacteria.

Interestingly, the TOC-normalized GDGT-0 concentration is higher at the depth of ~ 45–65 cm in the lake phase than that in the marsh phase. The peak of TOC-normalized GDGT-0 concentration also corresponds approximately to the peak alkenone concentrations in the lake phase (Fig. 4). GDGT-0 can be produced by both methanogenic and methanotrophic archaea as well as other archaea (reviewed by Schouten et al., 2013). Thus, our data suggest the relative productivities of GDGT-0-producing archaea are the highest when algal productivity is high in the lake phase. Even though the total organic carbon contents are high in the marsh phase, TOC-normalized concentrations of GDGT-0 are actually low. Therefore, organic matter quality (e.g., high algal production in the lake phase) rather than quantity (e.g., high vascular plant production in marsh phase) may be more important to the overall activities of GDGT-0-producing archaea relative to other organisms in the environment.

3.3. Cyclization of brGDGTs as indicator of Wudalianchi water pH changes

Cyclization indices of bacterial-derived brGDGTs (CBT and CBT′, Eqs. (5) and (6)) have been proposed as indicators of pH changes based on empirical correlations, with higher CBT values indicating lower pH, or higher CBT′ values indicating higher pH (Weijers et al., 2007; De Jonge et al., 2014). Here we explore whether CBT and CBT′ proxies record the drastic changes in pH resulting from the abrupt shift of environment from marsh to an alkaline lake. Marshes tend to have relatively low pH values, due to extensive organic matter decomposition in the low-oxygen to anaerobic, water-logged environment (Howarth and Hobbie, 1982). After the Laoheishan eruption, the efficient weathering and congruent dissolution of alkaline volcanic glass (e.g., silicate; Eq. (8); Sarin et al., 1989) and volcanic rock minerals (e.g., magnesium olivine; Eq. (9)) can release large amounts of HCO_3^- anion, rapidly raising the pH values of the lake water.

$$(\mathrm{K, Na, Mg, Ca})\text{silicate in tephra} + \mathrm{H_2CO_3} = \mathrm{HCO_3^-} + \mathrm{K^+} + \mathrm{Na^+} + \mathrm{Mg^{2+}} + \mathrm{Ca^{2+}} + \mathrm{H_4SiO_4} \quad (8)$$

$$\mathrm{Mg_2SiO_4(olivine)} + 4\mathrm{H_2CO_3} = 2\mathrm{Mg^{2+}} + 4\mathrm{HCO_3^-} + \mathrm{H_4SiO_4} \quad (9)$$

In our sediment core, CBT abruptly decreases from ~ 0.8 to 0.4 from the pre-eruption to early post-eruption phase, followed by a relatively constant value of ~ 0.35 in the post-eruption phase (Fig. 5a). CBT′ displays similar behavior in response to pH, with overall increasing trend from –0.69 to –0.13 (Fig. 5b). Our PCA result shows that brGDGT distributions in Wudalianchi sediment samples differ significantly from those from previously published regional soils within northeastern China (~40°–54° N; ~118°–135°E; Fig. 6; Xiao et al., 2015; Wang et al., 2016; Yao et al., 2020b). These data suggest that brGDGTs in the Wudalianchi sediments mainly originate from aquatic sources. Thus, the sedimentary brGDGT signals may primarily provide environmental information about the Wudalianchi catchment water. We employed the published lake CBT-pH calibration from Schoon et al. (2013) (pH = 10.24–3.45 × CBT) and CBT′-pH calibration from Russell et al. (2018) (pH = 8.95 + 2.65 × CBT′) to respectively calculate pH changes of the Wudalianchi catchment (Fig. 5c). From the pre-eruption phase to the post-eruption phase, the CBT-inferred pH values increase from an average of 7.6 to 9.0, and the CBT′-inferred pH values increase from an average of 7.2 to 8.4 (Fig. 5c; Supplementary Fig. S6a). The average CBT′-inferred pH 8.4 in the post-eruption phase is very close to modern measured lake water pH (8.6 in July 2016; Yao et al., 2019). The abrupt increases of ~ 1.2–1.4 following the volcanic eruption reflects alkaline glass dissolution and volcanic rock weathering. Notably, lake water pH stays at relatively high values throughout the post-eruption lake environment (Fig. 5c), indicating the long-lasting impact on water chemistry due to efficient weathering of alkaline basalt minerals and tephra. This is fully consistent with our element results (Fig. 2).

However, it should be noted that the CBT-inferred pH values from the Schoon et al. (2013) calibration are overall slightly higher than the CBT′-inferred pH from the Russell et al. (2018) calibration (Fig. 5c; Supplementary Fig. S6a). Considering the marsh environment of the Wudalianchi catchment prior to the volcanic eruption, we further calculated the pH in the pre-eruption phase based on the previously published peatland CBT′-pH calibration (pH = 9.19 + 2.69 × CBT′; Naafs et al., 2017). The inferred pH is slightly higher than that from the Russell et al. (2018) calibration, but is lower than that from the Schoon et al. (2013) calibration (Supplementary Fig. S6b). Further studies on a Wudalianchi-specific calibration based on sampling of suspended particulate matter from different water depth and seasons may help improve the accuracy of the reconstructed pH.

We also calculated the MBT'_{5Me} (Eq. 7) in the entire sediment core and inferred the mean temperature of months-above-freezing (MAF) using the most recent global Bayesian temperature calibration (Martínez-Sosa et al., 2021; Supplementary Fig. S7). The inferred temperature shows a decreasing trend from 13.9 °C to 8.8 °C in the post-eruption phase (Supplementary Fig. S7), which contradicts the well documented regional climate warming over the past ~ 130 years based on instrumental records (summarized in Yao et al., 2021). The inferred temperature (9.6 ℃) from the surface sediment is obviously colder than the instrumental MAF (13.8 ℃) in 2017 (our sediment core was collected in 2017). Temperature reconstruction using MBT'_{5Me} in Lake Wudalianchi may be complicated by the variable contributions of deeper water-derived brGDGTs as lake level fluctuates and changes in

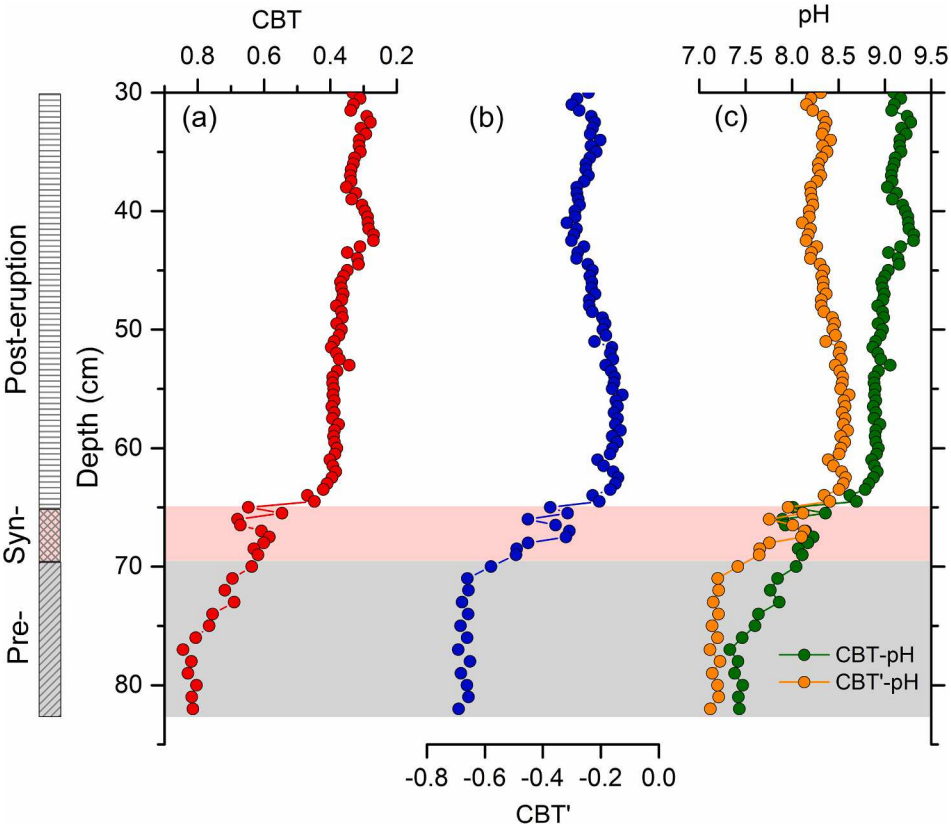

Fig. 5. Depth variations in CBT, CBT′, as well as CBT- and CBT′-inferred pH in our Lake Wudalianchi sediment core. The calibrations from Schoon et al. (2013) and Russell et al. (2018) are used to respectively calculate to pH. Grey shaded area represents pre-eruption period of depth range from 69 cm to 82 cm; Red shaded area represents *syn*-eruption phase from 65 cm to 69 cm depth. (For interpretation of the references to colour in this figure legend, the reader is referred to the web version of this article.)

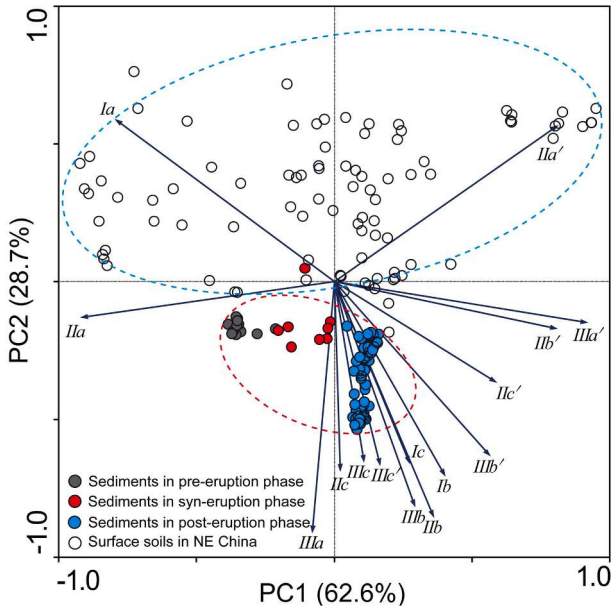

Fig. 6. Principal Component Analysis (PCA) showing the brGDGT distributions in our sediment core (including the pre-, syn- and post-eruption phases) and previously published surface soils of northeastern China (~40°–54° N; ~118°–135°E; Xiao et al., 2015; Wang et al., 2016; Yao et al., 2020b).

brGDGT-producing bacterial communities as redox condition varies (Yao et al., 2020b).

3.4. Group 1 alkenones for testing the inferred pH and oligohaline lake environment

Group 1 alkenones, exclusively produced by Group I Isochrysidales within haptophyte lineages, extensively occur in freshwater/oligohaline lakes throughout the mid- and high latitudes of the northern hemisphere (Longo et al., 2016, 2018; Wang et al., 2019; Yao et al., 2019). They are characterized by the presence of $\Delta^{14,21,28}$ tri-unsaturated isomer ($C_{37:3b}$) (Longo et al., 2016, 2018; Wang et al., 2019; Yao et al., 2019). The high concentration of Group 1 alkenones tends to occur in moderately alkaline (pH: ~7.3–8.8) freshwater lakes with an upper limit (~8.8) of pH (Yao et al., 2019). Such a preferred growing environment for Group 1 Isochrysidales can help test potential rationality of CBT- and CBT′-inferred pH in our Wudalianchi sediment record.

In our sediment core, Group 1 biomarker $C_{37:3b}$ and total C_{37} alkenones (including $C_{37:4}$, $C_{37:3a}$, $C_{37:3b}$, and $C_{37:2}$) were not detected in the pre-eruption and *syn*-eruption phases (Fig. 7a,b). After the volcanic eruption, Group 1 $C_{37:3b}$ and total C_{37} alkenones show up immediately (Fig. 7a,b). Their concentrations change synchronously (range of 0–287 ng/g for $C_{37:3b}$; range of 5–1425 ng/g for total C_{37}) and show the maximum at the depth of ~ 54 cm (Fig. 7a,b). The high $C_{37:3b}$ concentration occurs in the CBT′-inferred pH range of ~ 8.4–8.6 (Fig. 8a), which falls within the optimal range (~7.3–8.8) we previously proposed (Yao et al., 2019). However, the CBT-inferred pH with high $C_{37:3b}$ concentration samples are beyond the upper limit of (~8.8) for the growth of Group 1 Isochrysidales (Fig. 8b), indicating that the CBT-pH calibration from Schoon et al. (2013) may have overestimated pH of the lake water. We suggest that the CBT′-pH calibration from Russell et al. (2018) may be more suitable for reconstructing Wudalianchi pH changes.

Moreover, in the post-eruption phase, CBT-inferred pH values maximize at ~30–45 cm depth, whereas CBT′-inferred pH values

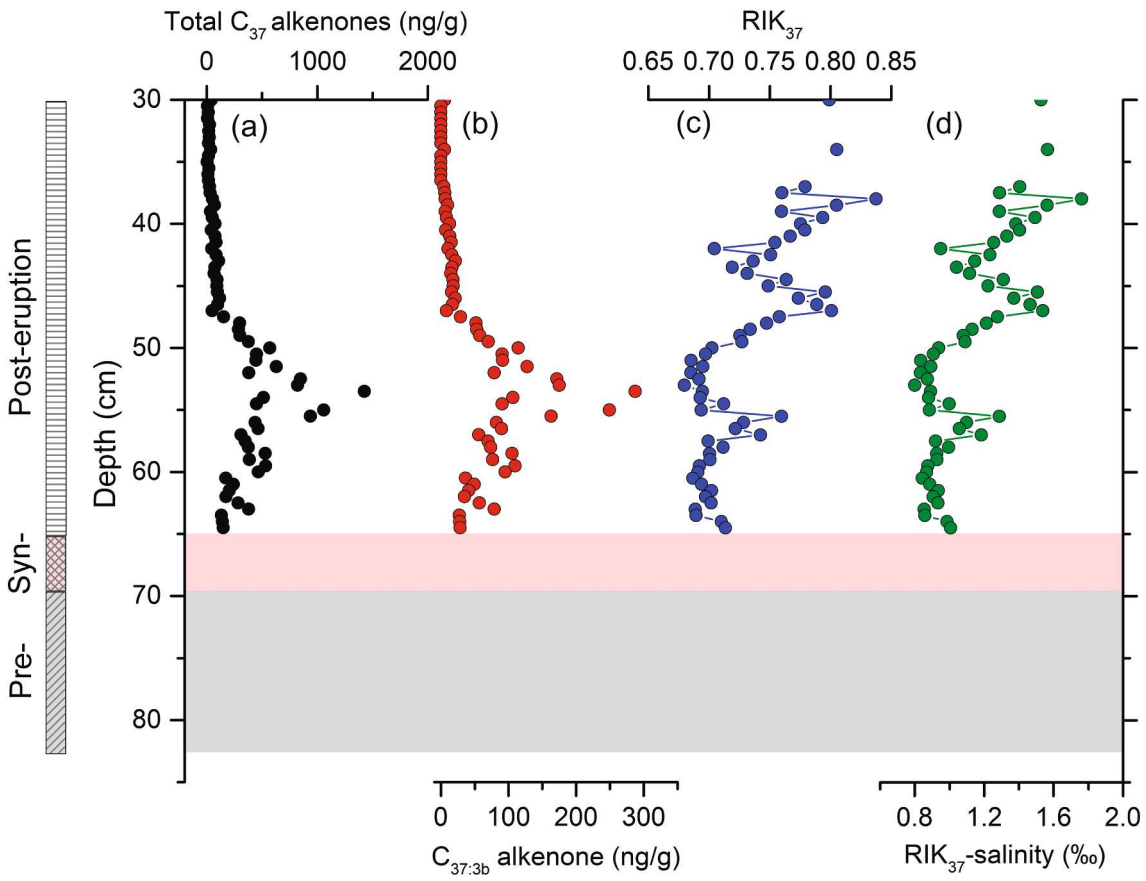

Fig. 7. Depth variations in total C_{37} alkenone concentration, $C_{37:3b}$ alkenone concentration (relative to sediment weight), as well as previously published RIK_{37} and RIK_{37}-inferred salinity (Yao et al., 2021). Grey shaded area represents pre-eruption period of depth range from 69 cm to 82 cm; Red shaded area represents *syn*-eruption phase from 65 cm to 69 cm depth. (For interpretation of the references to colour in this figure legend, the reader is referred to the web version of this article.)

maximize at ~50–60 cm depth (Fig. 5c). Downcore variations in $C_{37:3b}$ concentrations show a different relationship to those of CBT′- and CBT-inferred pH values. For example, peak $C_{37:3b}$ concentrations coincide with the highest CBT′-inferred pH values but correlate with intermediate CBT-inferred pH values (Fig. 5c and 7b). The CBT′-inferred pH values appear to be in better agreement with our previous observation that higher pH in moderately alkaline (pH: ~ 7.6–8.8) freshwater lakes generally facilitates greater production of Group 1 alkenones (Yao et al., 2019). We therefore suggest that CBT′ might be a better proxy for reconstructing lake water pH in alkaline environments. This may be because CBT′ includes mainly the pH-dependent 6-methyl brGDGTs in the numerator (De Jonge et al., 2014). The 6-methyl brGDGT isomers have been shown to increase in abundance as pH increases relative to their 5-methyl counterparts (e.g., De Jonge et al., 2014; Ding et al., 2015; Xiao et al., 2015; Yang et al., 2015). In high pH environments such as the lake phase in this study (CBT′-inferred pH of lake water is ~8.1–8.6; Fig. 5c), 6-methyl brGDGTs are often dominant over 5-methyl isomers (e.g., De Jonge et al., 2014; Ding et al., 2015; Xiao et al., 2015; Yang et al., 2015). Thus, in alkaline lake environments, CBT′ may provide more realistic reconstruction of past pH variations than CBT.

In lacustrine environments, in addition to Group 1 Isochrysidales occurring in freshwater/oligohaline lakes, another alkenone-producing Group 2 Isochrysidales extensively occur in global oligohaline and saline lakes (Theroux et al., 2010; Plancq et al., 2019; Yao et al., 2020a). With increasing salinity in oligohaline lakes, Group II Isochrysidales can gradually outcompete Group I Isochrysidales (Yao et al., 2020a). Thus, RIK_{37} based on the ratio of alkenone isomers $C_{37:3a}$ and $C_{37:3b}$ (Eq. (1)) can be used as a salinity proxy in freshwater and oligohaline environments (Kaiser et al., 2019; Yao et al., 2020a, 2021; Huang et al., 2021). Our recently published RIK_{37} values and inferred salinity in the same sediment core from Yao et al. (2021) indicate that Wudalianchi has been an oligohaline lake in the past ~ 240 years post volcanic eruption, with a salinity range of 0.8–1.76 ppt (Fig. 7c,d). The RIK_{37}-inferred lake water salinity shows significant fluctuations, whereas the CBT′-inferred pH is relatively constant after the volcanic eruption (Fig. 5c and 7d). Salinity fluctuations can be caused by changes in regional hydrological balances, evapotranspiration rates of vegetation as well as permafrost thawing (Yao et al., 2021). However, lake water pH in the post eruption phase is mainly dictated by tephra and basalt weathering processes and likely less sensitive to hydrological changes.

In such lake environments, GDGT-0/crenarchaeol ratios and MI values are significantly lower than those in the marsh environment before the volcanic eruption (Fig. 3c,d). These data indicate lower archaeal methanogenesis and methanotrophy in the post-eruption lake phase than the pre-eruption marsh phase. The difference in methanogenesis and methanotrophy between the two sedimentation units can be mainly attributed to the high organic carbon content (Fig. 3b) and strongly anaerobic conditions in the marsh phase.

4. Conclusions

Multiple lipid biomarker groups from a Lake Wudalianchi sediment core with a tephra layer provide highly detailed records of environmental and biogeochemical changes in aquatic ecosystem, hydrology, and methane cycling from the volcanic eruption in 1776. Before the volcanic eruption, our biomarker evidence of *n*-alkane P_{aq} and organic matter contents indicate a shallow organic-rich marsh environment with abundant emergent aquatic macrophytes in the Wudalianchi catchment. The combination of GDGT-0 concentrations, GDGT-0/crenarchaeol, MI, diploptene concentrations and $\delta^{13}C$ values indicates high microbial

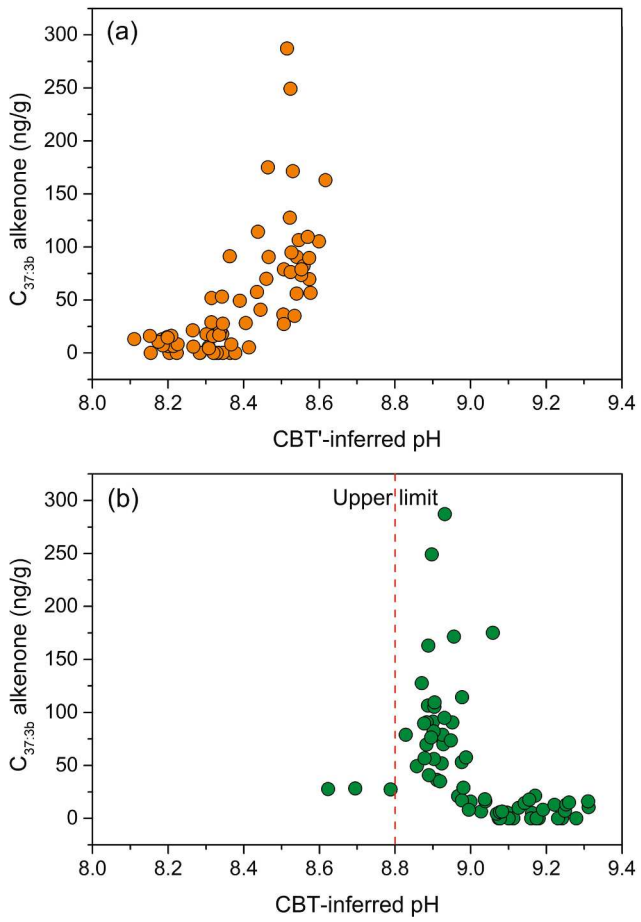

Fig. 8. $C_{37:3b}$ alkenone concentration vs. CBT- and CBT′-inferred pH in our Lake Wudalianchi sediment core.

activities of methanogenesis and methanotrophy in such environment.

After the volcanic eruption, the alkaline volcanic glass dissolution and volcanic rock weathering produces high alkalinity and led to a rapid increase in catchment water pH. The CBT and CBT′ responded abruptly and consistently to the pH changes and the inferred pH displays an abrupt increase of ~1.3. Meanwhile, the occurrence of Group 1 alkenones indicates that Wudalianchi became an oligohaline lake with moderately alkaline conditions. Our study demonstrates high efficacy of the lipid biomarker-based proxies for reconstructing pH, hydrology, and methane cycling, and presents a first example of long-lasting impacts of a volcanic eruption on aquatic ecosystems and associated biogeochemical cycling.

Declaration of Competing Interest

The authors declare that they have no known competing financial interests or personal relationships that could have appeared to influence the work reported in this paper.

Acknowledgements

This work was supported by the National Natural Science Foundation of China (No. 42073070; 41888101; 41702187), the U.S. National Science Foundation (Nos. EAR-1122749, PLR-1503846, EAR-1502455, EAR-1762431), and the Fundamental Research Funds for the Central Universities. YH thanks the Swiss Federal Institue of Technology for a visiting professorship and a senior fellowship at Collegium Helveticum in fall of 2021. We thank J.J. Jing and J. Chen for assistance during field sampling and pretreatment, Dr. G.Y. Sheng for diploptene identification, and J. Wu for discussion. We are also grateful for the comments from two anonymous reviewers, and editors Dr. John Volkman and Dr. Julian Sachs that helped us improve the manuscript.

Appendix A. Supplementary data

Supplementary data to this article can be found online at https://doi.org/10.1016/j.orggeochem.2021.104349.

References

Bao, K., Shen, J., Wang, G., Sapkota, A., McLaughlin, N., 2016. Estimates of recent Hg pollution in Northeast China using peat profiles from Great Hinggan Mountains. Environmental Earth Sciences 75, 536.
Bao, K., Zhang, Y., Zaccone, C., Meadows, M.E., 2021. Human impact on C/N/P/ accumulation in lake sediments from northeast China during the last 150 years. Environmental Pollution 271, 116345.
Blaga, C.I., Reichart, G.J., Heiri, O., Sinninghe Damsté, J.S., 2009. Tetraether membrane lipid distributions in water-column particulate matter and sediments: a study of 47 European lakes along a north-south transect. Journal of Paleolimnology 41, 523–540.
Borrel, G., Jézéquel, D., Biderre-Petit, C., Morel-Desrosiers, N., Morel, J., Peyret, P., Fonty, G., Lehours, A., 2011. Production and consumption of methane in freshwater lake ecosystems. Research in Microbiology 162, 832–847.
Bridgham, S.D., Cadillo-Quiroz, H., Keller, J.K., Zhuang, Q., 2013. Methane emissions from wetlands: biogeochemical, microbial, and modeling perspectives from local to global scales. Global Change Biology 19, 1325–1346.
Cao, J., Rao, Z., Jia, G., Xu, Q., Chen, F., 2017. A 15 ka pH record from an alpine lake in north China derived from the cyclization ratio index of aquatic brGDGTs and its paleoclimatic significance. Organic Geochemistry 109, 31–46.
Carpenter, S.R., Stanley, E.H., Vander Zanden, M.J., 2011. State of the world's freshwater ecosystems: physical, chemical, and biological changes. Annual Review of Environment and Resources 36, 75–99.
Castañeda, I.S., Schouten, S., 2011. A review of molecular organic proxies for examining modern and ancient lacustrine environments. Quaternary Science Reviews 30, 2851–2891.
Chen, J., 1994. Dedu County History: Nanjing. Huangshan Press (in Chinese).
Chen, X., Liu, X., Wei, Y., Huang, Y., 2019. Production of long-chain *n*-alkyl lipids by heterotrophic microbes: New evidence from Antarctic lakes. Organic Geochemistry 138, 103909.
Chen, X., Liu, X., Jia, H., Jin, J., Kong, W., Huang, Y., 2021. Inverse hydrogen isotope fractionation indicates heterotrophic microbial production of long-chain *n*-alkyl lipids in desolate Antarctic ponds. Geobiology 19, 394–404.
Cross, J.K., Tomlinson, E.L., Giordano, G., Smith, V.C., De Benedetti, A.A., Roberge, J., Manning, C.J., Wulf, S., Menzies, M.A., 2014. High level triggers for explosive mafic volcanism: Albano Maar, Italy. Lithos 190–191, 137–153.
De Jonge, C., Hopmans, E.C., Zell, C.I., Kim, J.-H., Schouten, S., Sinninghe Damsté, J.S., 2014. Occurrence and abundance of 6-methyl branched glycerol dialkyl glycerol tetraethers in soils: implications for palaeoclimate reconstruction. Geochimica et Cosmochimica Acta 141, 97–112.
Ding, S., Xu, Y., Wang, Y., He, Y., Hou, J., Chen, L., He, J., 2015. Distribution of branched glycerol dialkyl glycerol tetraethers in surface soils of the Qinghai-Tibetan Plateau: implications of brGDGTs-based proxies in cold and dry regions. Biogeosciences 12, 3141–3151.
Elvert, M., Pohlman, J.W., Becker, K.W., Gaglioti, B., Hinrichs, K.-U., Wooller, M.J., 2016. Methane turnover and environmental change from Holocene lipid biomarker records in a thermokarst lake in Arctic Alaska. The Holocene 26, 1766–1777.
Ficken, K.J., Li, B., Swain, D.L., Eglinton, G., 2000. An *n*-alkane proxy for the sedimentary input of submerged/floating freshwater aquatic macrophytes. Organic Geochemistry 31, 745–749.
Hopmans, E.C., Schouten, S., Sinninghe Damsté, J.S., 2016. The effect of improved chromatography on GDGT-based palaeoproxies. Organic Geochemistry 93, 1–6.
Howarth, R.W., Hobbie, J.E., 1982. In: The regulation of decomposition and heterotrophic microbial activity in salt marsh soils: a review. Academic Press, pp. 183–207.
Huang, Y., Zheng, Y., Heng, P., Giosan, L., Coolen, M.J.L., 2021. Black Sea paleosalinity evolution since the last deglaciation reconstructed from alkenone-inferred Isochrysidales diversity. Earth and Planetary Science Letters 564, 116881.
Inglis, G.N., Naafs, B.D.A., Zheng, Y., Schellekens, J., Pancost, R.D., the T-GRES peat database collaborators, 2019. $\delta^{13}C$ values of bacterial hopanoids and leaf waxes as tracers for methanotrophy in peatlands. Geochimica et Cosmochimica Acta 260, 244–256.
Johnson, N., Revenga, C., Echeverria, J., 2001. Managing water for people and nature. Science 292, 1071–1072.
Kaiser, J., Wang, K.J., Rott, D., Li, G., Zheng, Y., Amaral-Zettler, L., Arz, H.W., Huang, Y., 2019. Changes in long chain alkenone distributions and Isochrysidales groups along the Baltic Sea salinity gradient. Organic Geochemistry 127, 92–103.
Karger, D.N., Conrad, O., Böhner, J., Kawohl, T., Kreft, H., Soria-Auza, R.W., Zimmermann, N.E., Linder, H.P., Kessler, M., 2017. Climatologies at high resolution for the earth's land surface areas. Scientific Data 4, 170122.
Kilian, R., Biester, H., Behrmann, J., Baeza, O., Fesq-Martin, M., Hohner, M., Schimpf, D., Friedmann, A., Mangini, A., 2006. Millennium-scale volcanic impact on a superhumid and pristine ecosystem. Geology 34, 609–612.

Kuritani, T., Kimura, J., Ohtani, E., Miyanoto, H., Furuyama, K., 2013. Transition zone origin of potassic basalts from Wudalianchi volcano, northeast China. Lithos 156–159, 1–12.
Lehner, B., Döll, P., 2004. Development and validation of a global database of lakes, reservoirs and wetland. Journal of Hydrology 296, 1–22.
Liu, J., Wang, Z., Zhao, H., Peros, M., Yang, Q., Liu, S., Li, H., Wang, S., Bu, Z., 2018. Mercury and arsenic in the surface peat soils of the Changbai Mountains, northeastern China: distribution, environmental controls, sources, and ecological risk assessment. Environmental Science and Pollution Research 25, 34595–34609.
Longo, W.M., Theroux, S., Gibin, A.E., Zheng, Y., Dillon, J.T., Huang, Y., 2016. Temperature calibration and phylogenetically distinct distributions for freshwater alkenones: Evidence from northern Alaskan lakes. Geochimica et Cosmochimica Acta 180, 177–196.
Longo, W.M., Huang, Y., Yao, Y., Zhao, J., Giblin, A.E., Wang, X., Zech, R., Haberzettl, T., Jardillier, L., Toney, J., Liu, Z.H., Krivonogov, S., Kolpakova, M., Chu, G.Q., D'Andrea, W.J., Harada, N., Nagashima, K., Sato, M., Yonenobu, H., Yamada, K., Gotanda, K., Shinozuka, Y., 2018. Widespread occurrence of distinct alkenones from Group I haptophytes in freshwater lakes: Implications for paleotemperature and paleoenvironmental reconstructions. Earth and Planetary Science Letters 492, 239–250.
Lyu, M., Sheng, L., Zhang, Z., Zhang, L., 2016. Distribution and accumulation of soil carbon in temperate wetland, Northeast China. Chinese Geographical Science 26, 295–303.
Mackenzie, L., Bao, K., Mao, L., Klamt, A., Pratte, S., Shen, J., 2018. Anthropogenic and climate-driven environmental change in the Songnen Plain of northeastern China over the past 200 years. Palaeogeography, Palaeoclimatology, Palaeoecology 511, 208–217.
Markovic, D., Carrizo, S.F., Kärcher, O., Walz, A., David, J.N.W., 2017. Vulnerability of European freshwater catchments to climate change. Global Change Biology 23, 3567–3580.
Martínez-Sosa, P., Tierney, J.E., Stefanescu, I.C., Crampton-Flood, E.D., Shuman, B.N., Routson, C., 2021. A global Bayesian temperature calibration for lacustrine brGDGTs. Geochimica et Cosmochimica Acta 305, 87–105.
Maruyama, S., Hattori, K., Hirata, T., Danhara, T., 2016. A proposed methodology for analyses of wide-ranged elements in volcanic glass shards in widespread Quaternary tephras. Quaternary International 397, 267–280.
McGee, L.E., McLeod, C., Davidson, J.P., 2015. A spectrum of disequilibrium melting preserved in lava-hosted, partially melted crustal xenoliths from the Wudalianchi volcanic field, NE China. Chemical Geology 417, 184–199.
Megonigal, J.P., 2002. Methane-limited methanotrophy in tidal freshwater swamps. Global Biogeochemical cycles 16, 1088.
Melson, W.G., O'Hearn, T., Jarosewich, E., 2002. A data brief on the Smithsonian Abyssal Volcanic Glass Data File. Geochemistry Geophysics Geosystems 3, 1–11.
Naafs, B.D.A., Inglis, G.N., Zheng, Y., Amesbury, M.J., Biester, H., Bindler, R., Blewett, J., Burrows, M.A., del Castillo Torres, D., Chambers, F.M., Cohen, A.D., Evershed, R.P., Feakins, S.J., Galka, M., Gallego-Sala, A., Gandois, L., Gray, D.M., Hatcher, P.G., Honorio Coronado, E.N., Hughes, P.D.M., Huguet, A., Könönen, M., Laggoun-Défarge, F., Lähteenoja, O., Lamentowicz, M., Marchant, R., McClymont, E., Pontevedra-Pombal, X., Ponton, C., Pourmand, A., Rizzuti, A.M., Rochefort, L., Schellekens, J., De Vleeschouwer, F., Pancost, R.D., 2017. Introducing global peat-specific temperature and pH calibrations based on brGDGT bacterial lipids. Geochimica et Cosmochimica Acta 208, 285–301.
Naeher, S., Niemann, H., Peterse, F., Smittenberg, R.H., Zigah, P.K., Schubert, C.J., 2014. Tracing the methane cycle with lipid biomarkers in Lake Rotsee (Switzerland). Organic Geochemistry 66, 174–181.
Pancost, R.D., Sinninghe Damsté, J.S., 2003. Carbon isotopic compositions of prokaryotic lipids as tracers of carbon cycling in diverse settings. Chemical Geology 195, 29–58.
Payne, R.J., Egan, J., 2019. Using palaeoecological techniques to understand the impacts of past volcanic eruptions. Quaternary International 499, 278–289.
Plancq, J., Couto, J.M., Ijaz, U.Z., Leavitt, P.R., Toney, J.L., 2019. Next-generation sequencing to identify lacustrine haptophytes in the Canadian Prairies: significance for temperature proxy applications. Journal of Geophysical Research: Biogeosciences 124, 2144–2158.
Reay, D.S., Smith, P., Christensen, T.R., James, R.H., Clark, H., 2018. Methane and global environmental change. Annual Review of Environment and Resources 43, 165–192.
Russell, J.M., Hopmans, E.C., Loomis, S.E., Liang, J., Sinninghe Damsté, J.S., 2018. Distributions of 5- and 6-methyl branched glycerol dialkyl glycerol tetraethers (brGDGTs) in East African lake sediments: Effects of temperature, pH, and new lacustrine paleotemperature calibrations. Organic Geochemistry 117, 56–69.
Sarin, M.M., Krishnaswami, S., Dilli, K., Somayajulu, B.L.K., Moore, W.S., 1989. Major ion chemistry of the Ganga-Brahmaputra river system: Weathering processes and fluxes to the Bay of Bengal. Geochimica et Cosmochimica Acta 53, 997–1009.
Schoon, P.L., de Kluijver, A., Middelburg, J.J., Downing, J.A., Sinninghe Damsté, J.S., Schouten, S., 2013. Influence of lake water pH and alkalinity on the distribution of core and intact polar branched glycerol dialkyl glycerol tetraethers (GDGTs) in lakes. Organic Geochemistry 72–82.
Schouten, S., Hopmans, E.C., Sinninghe Damsté, J.S., 2013. The organic geochemistry of glycerol dialkyl glycerol tetraether lipids: a review. Organic Geochemistry 54, 19–61.
Siebert, L., Simkin, T., 2013. Volcanoes of the World: An Illustrated Catalog of Holocene Volcanoes and their Eruptions, www.volcano.si.edu.
Sun, C., Németh, K., Zhan, T., You, H., Chu, G., Liu, J., 2019. Tephra evidence for the most recent eruption of Laoheishan volcano, Wudalianchi volcanic field, northeast China. Journal of Volcanology and Geothermal Research 383, 103–111.
Theroux, S., D'Andrea, W.J., Toney, J., Amaral-Zettler, L., Huang, Y., 2010. Phylogenetic diversity and evolutionary relatedness of alkenone-producing haptophyte algae in lakes: Implications for continental paleotemperature reconstructions. Earth and Planetary Science Letters 300, 311–320.
Tierney, J.E., Russell, J.M., 2009. Distributions of branched GDGTs in a tropical lake system: Implications for lacustrine application of the MBT/CBT paleoproxy. Organic Geochemistry 40, 1032–1036.
Tomlinson, E.L., Smith, V.C., Albert, P.G., Aydar, E., Civetta, L., Raffaello, C., Çubukçu, E., Gertisser, R., Isaia, R., Menzies, M.A., Orsi, G., Rosi, M., Zanchetta, G., 2015. The major and trace element glass compositions of the productive Mediterranean volcanic sources: tools for correlating distal tephra layers in and around Europe. Quaternary Science Reviews 118, 48–66.
Tyler, J.J., Nederbragt, A.J., Jones, V.J., Thurow, J.W., 2010. Assessing past temperature and soil pH estimates from bacterial and tetraether membrane lipids: Evidence from the recent lake sediments of Lochnagar. Scotland. Journal of Geophysical Research 115, G01015.
Vis, C., Hudon, C., Carignan, R., 2003. An evaluation of approaches used to determine the distribution and biomass of emergent and submerged aquatic macrophytes over large spatial scales. Aquatic Botany 77, 187–201.
Wang, H., Liu, W., Lu, H., 2016. Appraisal of branched glycerol dialkyl glycerol tetraether-based indices for North China. Organic Geochemistry 98, 118–130.
Wang, K.J., O'Donnell, J.A., Longo, W.M., Amaral-Zettler, L., Li, G., Yao, Y., Huang, Y., 2019. Group I alkenones and Isochrysidale in the world's largest maar lakes and their potential paleoclimate applications. Organic Geochemistry 138, 103924.
Weijers, J.W.H., Schouten, S., van den Donker, J.C., Hopmans, E.C., Sinninghe Damsté, J. S., 2007. Environmental controls on bacterial tetraether membrane lipid distribution in soils. Geochimica et Cosmochimica Acta 71, 703–713.
Xiao, W., Xu, Y., Ding, S., Wang, Y., Zhang, X., Yang, H., Wang, G., Hou, J., 2015. Global calibration of a novel, branched GDGT-based soil pH proxy. Organic Geochemistry 89–90, 56–60.
Yang, H., Lü, X., Ding, W., Lei, Y., Dang, X., Xie, S., 2015. The 6-methyl branched tetraethers significantly affect the performance of the methylation index (MBT) in soils from an altitudinal transect at Mount Shennongjia. Organic Geochemistry 82, 42–53.
Yao, Y., Zhao, J., Longo, W.M., Li, G., Wang, X., Vachula, R.S., Wang, K.J., Huang, Y., 2019. New insights into environmental controls on the occurrence and abundance of Group I alkenones and their paleoclimate applications: Evidence from volcanic lakes of northeastern China. Earth and Planetary Science Letters 527, 115792.
Yao, Y., Lan, J., Zhao, J., Vachula, R.S., Xu, H., Cai, Y., Cheng, H., Huang, Y., 2020a. Abrupt freshening since the early Little Ice Age in Lake Sayram of arid central Asia inferred from an alkenone isomer proxy. Geophysical Research Letters 47 e2020GL089257.
Yao, Y., Zhao, J., Vachula, R.S., Werne, J.P., Wu, J., Song, X., Huang, Y., 2020b. Correlation between the ratio of 5-methyl hexamethylated to pentamethylated branched GDGTs (HP5) and water depth reflects redox variations in stratified lakes. Organic Geochemistry 147, 104076.
Yao, Y., Huang, Y., Zhao, J., Wang, L., Ran, Y., Liu, W., Cheng, H., 2021. Permafrost thaw induced abrupt changes in hydrology and carbon cycling in Lake Wudalianchi, northeastern China. Geology 49, 1117–1121.
Zhang, Y.G., Zhang, C.L., Liu, X.L., Li, L., Hinrichs, K.U., Noakes, J.E., 2011. Methane Index: A tetraether archaeal lipid biomarker indicator for detecting the instability of marine gas hydrates. Earth and Planetary Science Letters 307, 525–534.
Zheng, Y., Singarayer, J.S., Cheng, P., Yu, X., Liu, Z., Valdes, P.J., Pancost, R.D., 2014. Holocene variations in peatland methane cycling associated with the Asian summer monsoon system. Nature Communications 5, 4631.
Zheng, Y., Tarozo, R., Huang, Y., 2017. Optimizing chromatographic resolution for simultaneous quantification of long chain alkenones, alkenoates and their double bond positional isomers. Organic Geochemistry 111, 136–143.